A simulation of bromoform's contribution to stratospheric bromine

J. Eric Nielsen[1]

Emergent Information Technologies, Inc., Vienna, Virginia

Anne R. Douglass

NASA Goddard Space Flight Center, Greenbelt, Maryland

Short title: BROMOFORM AND STRATOSPHERIC BROMINE

Abstract.

Many chlorinated and brominated compounds that are inert in the troposphere are destroyed in the stratosphere and act as an in-situ source of stratospheric reactive chlorine and bromine. Other halogenated compounds that are reactive in the troposphere might contribute to the stratosphere's halogen budget in two ways. First, like their unreactive companions, rapid convective transport might carry them to the upper troposphere and make them available for subsequent advection by the mean circulation into the stratosphere before they are oxidized or photolyzed. Second, it is more likely that they are destroyed in the troposphere, and the chlorine and bromine that is released might then be transported to the stratosphere. We evaluate the relative influence of these processes on stratospheric bromine in a three-dimensional chemistry and transport model which simulates the distribution of bromoform ($CHBr_3$). $CHBr_3$ is parameterized as a short-lived, ocean-surface source gas whose destruction by photolysis and reaction with hydroxyl (OH) in the troposphere and stratosphere yields inorganic bromine (Br_y). Many of the observed features of $CHBr_3$ are simulated well, and comparisons with observations are used to show that the model represents aspects of transport in the upper troposphere and lower stratosphere that are critical to the evaluation. In particular, the model maintains the observed troposphere-stratosphere distinctness in transport pathways and reproduces the observed seasonal dependence of the mixture of air in the middle- and high-latitude lowermost stratosphere. We estimate that adding $CHBr_3$ to models which already include the long-lived organic brominated compounds (halons and methyl bromide) will increase the simulated stratospheric mass of Br_y by about 15%. In-situ stratospheric destruction of $CHBr_3$ produces Br_y in amounts which are comparable to that transported into the stratosphere after photolysis and oxidation of $CHBr_3$ in the troposphere. In our simulations the mass of Br_y produced from the destruction of $CHBr_3$ does not exceed the mass of Br_y produced from the destruction of the long-lived compounds at any level in the stratosphere. However, Br_y from the loss of $CHBr_3$ accounts for approximately one-third of the total Br_y in the lowest kilometer of the stratosphere.

1. Introduction

Organic brominated and chlorinated compounds are the primary sources of stratospheric bromine and chlorine. These gases are released at the ground through both natural and anthropogenic processes, and their lifetimes are as widely varying as their molecular compositions. The long-lived compounds, with lifetimes of many months or years, are nonreactive in the troposphere and are transported to the stratosphere where they are subject to photolysis and reaction with radicals. The bromine or chlorine that is released then becomes bound into one of several molecules that comprise inorganic bromine (Br_y) or inorganic chlorine (Cl_y), respectively. These molecules are known to participate in catalytic reactions which accelerate ozone destruction in the stratosphere [*WMO*, 1999], so an accurate assessment of the stratospheric burden of Br_y and Cl_y is of interest. The major long-lived organic brominated compounds are the halons (H-1211, $CBrClF_2$; H-1301, $CBrF_3$; H-2402, $C_2Br_2F_4$) and methyl bromide (CH_3Br).

Short-lived compounds, with lifetimes on the order of days or weeks are oxidized or photolyzed primarily in the troposphere. Only small amounts are transported to the lower stratosphere, so the in-situ stratospheric release of their bromine and chlorine is not thought to substantially contribute to the stratospheric burden. But the inorganic bromine and chlorine released in the troposphere may be transported to the stratosphere as well and, as postulated by *Ko et al.* [1997], may represent an additional source of stratospheric Br_y and Cl_y which is not comprehensively addressed by global atmospheric chemistry models.

The first global modeling study to concentrate on the short-lived species' contribution to stratospheric Br_y is detailed by *Dvortsov et al.* [1999]. They use the off-line version of the CCM3 Model of Atmospheric Transport and Chemistry (MATCH) [*Rasch et al.*, 1997] to simulate bromoform ($CHBr_3$), the most abundant short-lived organic brominated species in the boundary layer [*WMO*, 1999], and dibromomethane (CH_2Br_2) in the troposphere. MATCH provides a lower boundary condition for a two-dimensional (zonally averaged) simulation that includes the stratosphere [*Smyshlyaev et al.*, 1998]. Br_y is produced by photolysis and oxidation of the two source gases. The Br_y which comes from destruction of $CHBr_3$ is generated mostly within the troposphere and also in the stratosphere below 19

km. *Dvortsov et al.* [1999] conclude that $CHBr_3$ accounts for more Br_y in the lowermost stratosphere than is produced from all the long-lived sources combined.

The objective of this study is to provide a similar assessment of the contribution of $CHBr_3$ to stratospheric Br_y. Since the short-lived species are constrained by their photolysis and oxidation characteristics to make their largest relative contribution to stratospheric bromine in the lowest regions of the stratosphere, it is important to accurately resolve transport processes near the tropopause. This is a major focus of our methodology which differs in two ways from that of *Dvortsov et al.* [1999]. First, we execute both the tropospheric and stratospheric parts of our simulations in three dimensions with transport driven by assimilated winds. This enables us to globally map the tropopause and to consistently separate the troposphere from the stratosphere in the simulations and the diagnostic analyses. Second, we parameterize the chemistry of $CHBr_3$ and of the Br_y which is produced by its destruction, but use a separate three-dimensional global photochemical model to simulate the long-lived organic brominated compounds and their byproducts. While we acknowledge that execution of the models is done separately and that the vertical discretization of the full-chemistry model is necessarily more coarse, both models use the same assimilated data and the same transport numerics. Hence the assessment is performed on simulated Br_y from two models which have nearly equivalent representations of the both the transport and the tropopause.

Our analysis includes diagnostics which assess the models' ability to reproduce the observed transport processes in the upper troposphere and lowermost stratosphere. The lowermost stratosphere is the region bounded below by the tropopause and above by the 380 K potential temperature surface [*Holton, et al.*, 1995; *Appenzeller et al.*, 1996]. Recent studies [*Ray et al.*, 1999; *Hintsa et al.*, 1998; *Dessler et al.*, 1995] show that the lowermost stratosphere contains a seasonally varying mixture of air from the tropical upper troposphere and from the so-called stratospheric overworld which lies above the 380 K potential temperature surface. In particular, *Ray et al.* [1999] use measurements of photolytic species to show that cumulative downward vertical advection from the stratospheric overworld determines mixing ratios in May and cumulative quasi-horizontal, isentropic advection from

the tropical upper troposphere determines the mixing ratios in September. That is, air with origins in the tropical upper troposphere dominates the middle-latitude lowermost stratosphere at the end of summer while air from the overworld dominates at the end of winter. During winter the subtropical jet presents a barrier to quasi-isentropic, cross-tropopause transport and Rossby and gravity waves generate downward transport at the base of the middle- and high-latitude overworld. In summer, this barrier to isentropic transport is weak and the tropospheric monsoon circulations drive the quasi-horizontal upper troposphere to lower stratosphere exchange [*Dunkerton*, 1995; *Chen*, 1995]. Ray et al.'s [1999] Figure 3 illustrates the resulting seasonal variation for CFC-11 (CCl_3F) at 34° N in the lowermost stratosphere. $CHBr_3$ should display a similarly strong seasonal cycle in the northern middle-latitude lowermost stratosphere since its photolytic characteristics, like those of CFC-11, yield relatively high mixing ratios in the upper tropical troposphere compared to mixing ratios near zero in the middle and upper stratosphere. Since we are assessing the relative contributions to stratospheric Br_y from the destruction of $CHBr_3$ in both the troposphere and stratosphere, the validity of the simulations rests on a model's ability to preserve the seasonality of these two different pathways by which air enters the extratropical middle-latitude lowermost stratosphere.

The numerical models and the parameterized chemistry are detailed in the next section. In Section 3, we present the results of the $CHBr_3$ simulation and demonstrate that the assimilated winds reproduce the observed seasonal change in the mixture of air in the lowermost stratosphere. This provides confidence in our assessment of $CHBr_3$'s contribution to stratospheric Br_y. Section 4 provides a short summary and conclusions.

2. Description of the experiments

2.1. Models and dynamics

Our simulations of $CHBr_3$ and the Br_y produced from destruction of $CHBr_3$ are performed with the parameterized chemistry and transport model (PCTM) from the Laboratory for Atmospheres at Goddard Space Flight Center. This model successfully reproduces many of the observed features of the

distribution of ozone [*Douglass et al.*, 1996, *Rood et al.*, 2000], carbon dioxide (CO_2) [*Strahan et al.*, 1998], and water vapor [*Gettelman et al.*, 2000]. The PCTM includes a flux-form, semi-Lagrangian transport algorithm described by [*Lin and Rood*, 1996]. It is run in the off-line mode with winds, temperatures, and surface pressures provided by the Goddard Earth Observing System Data Assimilation System (GEOS-DAS) [*Schubert et al.*, 1993]. The GEOS-DAS dynamics are available at six-hour intervals and are temporally interpolated to each 15-minute PCTM time step. The starting date is January 1 and the PCTM is integrated through four years. Assimilated data from 1997 are recycled for each year of the experiment, so there is no element of interannual variability in the dynamics. The PCTM's grid boxes occupy $2\frac{1}{2}^\circ$ longitude by 2° latitude, and the vertical domain extends from the ground to 0.121 hPa. The hybrid terrain-following and isobaric vertical coordinate has an interface pressure of 337 hPa. There are 37 layers, five in the terrain-following region and 32 in the isobaric region. The depth of the PCTM's 15 layers in the upper troposphere and lower stratosphere, from 50 to 337 hPa, is approximately 800 meters each. In the remainder of the troposphere and stratosphere the depth of the grid boxes are 1.3 km and 2.5 km, respectively. The region of finest vertical discretization is provided to enhance resolution of cross-tropopause transport.

The GEOS-DAS uses a relaxed Arakawa-Schubert scheme to parameterize subgrid-scale clouds, and the PCTM uses the diagnosed cloud mass flux and detrainment to drive a parameterization of "apparent momentum" transport by clouds based on *Schneider and Lindzen* [1976]. The results of a PCTM experiment without convective transport (not shown) verify that a parameterization of convection is necessary to transport $CHBr_3$ to the upper troposphere rapidly enough to overcome its short tropospheric lifetime [*Ko et al.*, 1997], especially in the tropics. In the lower stratosphere, however, the larger-scale circulation is sufficient to describe the behavior of certain constituents. This is shown by the tracer simulations referenced in the previous paragraph, none of which invoked a parameterization of convective transport. In particular, *Strahan et al.* [1998] use aircraft data to show that the amplitude of the CO_2 annual cycle in the lower stratosphere is much weaker than in the upper troposphere and that the stratospheric signal peaks approximately one to two months following the

upper tropospheric maximum. Neither of these features of the annual cycle can be attributed to vertical transport directly across the tropopause into the stratosphere, but instead are argued to both be a result of relatively fast, quasi-horizontal transport along isentropes from the tropical upper troposphere through the tropopause into the lowermost stratosphere. *Strahan et al.* [1998] use the PCTM and GEOS-DAS dynamics to simulate this troposphere-stratosphere distinctness in the transport of CO_2, but do not include convection.

Since the seasonal cycle of long-lived constituents in the middle- and high-latitude lowermost stratosphere must arrive quasi-isentropically via the tropical tropopause, convective transport at the scales of motion resolvable in this study must not in general penetrate into the stratosphere, at least to the extent that it can interfere with the signal propagation. To demonstrate that this is the case with the PCTM, we perform a two-year CO_2 simulation in tandem with the first two years of the $CHBr_3$ simulation. This experiment is similar to that of *Strahan et al.* [1998], and the evolution of the CO_2 annual cycle in the upper troposphere and lower stratosphere at 60° N latitude is shown in Figure 1 for the second year of the simulation. The amplitude of the annual cycle is much weaker in the stratosphere and the arrival of the maximum is delayed by approximately two months. This compares well to Figure 8 from *Strahan et al.* [1998] and Figure 6 from *Hall and Prather* [1993] and demonstrates that the addition of convection to the PCTM is not adversely affecting long-lived tracer transport in the middle- and high-latitude lowermost stratosphere. The PCTM satisfies an objective test of this apparent separation of the troposphere and stratosphere provided by *Douglass et al.* [1999].

The PCTM is not suitable for modeling the destruction of the long-lived organic brominated compounds and their byproducts. Instead the simulation of these compounds and the stratospheric Br_y which is produced from their destruction is provided by the Goddard full chemistry and transport model (FCTM). The FCTM is described by *Douglass and Kawa* (1999) and includes all gas phase reactions and six heterogeneous reactions thought to be important in the stratosphere. The FCTM is integrated from March 20, 1997 through January 1, 1998 using the same flux-form semi-Lagrangian transport alogorithm and the same 1997 GEOS-DAS dynamics which are used in the PCTM simulations. The

chemical initialization for the long-lived species and families in the FCTM is generated following *Douglass, et al.* [1997] using zonally averaged fields from the Goddard two-dimensional chemistry and transport model (2DCTM) [*Fleming et al.*, 1999] which has been integrated to steady state. *WMO* [1999] specifies the surface concentrations of the long-lived compounds used in both the FCTM and the 2DCTM, and in lieu of a detailed hydrological cycle, each of these compounds is subject to tropospheric scavenging with time scales of approximately 1 day at the surface and greater than 100 days at the tropopause. While the horizontal grid in the FCTM is identical to that in the PCTM, the vertical discretization of the FCTM is less dense, and the FCTM does not invoke the parameterization of convective transport. To obtain stratospheric Br_y from the FCTM, Br, BrO, HBr, HOBr, BrCl, and $BrONO_2$ are summed. Each compound is vertically interpolated onto the PCTM's vertical grid for diagnosis and comparison.

2.2. Parameterized chemistry

The PCTM solves the constituent continuity equation by process splitting [*Rood*, 1987; *McRea et al.*, 1982]. During each time step, advection is first applied to each constituent. This produces an "intermediate" constituent distribution, χ^*. Then the photochemical parameterization is incorporated by solving [*Douglass et al.*, 1989, *Rood et al.*, 1991]

$$\chi(t + \Delta t) = (\chi^* + P\Delta t) / (1 + L\Delta t),$$

where χ is the constituent mixing ratio, t is time, Δt is the time step length, P is the rate of production of χ, and L is the loss frequency of χ. The formulation of P and L for both $CHBr_3$ and Br_y is described below. The initial condition contains no $CHBr_3$ or Br_y.

2.2.1. Bromoform. $CHBr_3$ is treated as an ocean surface source gas that is destroyed by photolysis and reaction with hydroxyl (OH) in the troposphere and stratosphere. Various algal species are responsible for the natural production of $CHBr_3$ [*WMO*, 1999; *Sturges et al.*, 1992; *Gschwend et al.*, 1985]. In part because the distribution of algae in seawater is variable, the surface source strength is uncertain and difficult to assess [*WMO*, 1999]. Estimates range from 8×10^7 kg yr^{-1} to 2×10^9 kg yr^{-1}

[*Moore et al.*, 1993; *Liss et al.*, 1986; *Penkett et al.*, 1983]. For simplicity, we inject $CHBr_3$ into the atmosphere uniformly in space and time from the ocean surface at the rate S kg yr^{-1}. The production rate in molecules per second, P, in each grid box whose lower surface contacts the ocean is

$$P = \frac{-gN_A}{R_* T} \frac{M_a}{M_{CHBr_3}} \frac{S}{\Delta \ln p},$$

where g is the earth's gravity (9.8 m s^{-2}), N_A is Avogadro's number (6.022×10^{26} kmol^{-1}), R_* is the universal gas constant (8.3143×10^3 J kmol^{-1} K^{-1}), T is temperature, $\Delta \ln p$ is the pressure depth of the grid box, and M_a/M_{CHBr_3} is the ratio of the molecular weight of dry air (28.9 kg kmol^{-1}) to that of bromoform (253 kg kmol^{-1}). In all other grid boxes, $P = 0$. S is set to 5×10^8 kg yr^{-1} in an attempt to generate the observed tropical tropospheric $CHBr_3$ mixing ratios [*Schauffler et al.*, 1999]. Our S is 1.67 times that used by *Dvortsov et al.* [1999].

The sinks for $CHBr_3$ are photolysis and oxidation by OH. The loss frequency for the latter is derived from the rate constant given by *DeMore et al.* [1997] multiplied by the local concentration of OH, [OH]. Daytime averages of both the photolysis loss frequency, J, and [OH] are taken from the Goddard 2DCTM. In the PCTM, their local values are determined by weighting their respective daytime averages by the ratio of the cosine of the local solar zenith angle to the cosine of its daytime average. This ensures that [OH] and J will be zero at night and largest when the solar zenith angle is at its minimum. Figure 2 provides a comparison of the derived [OH] to the climatology from *Spivakovsky et al.* [2000]. Except in the few PCTM layers nearest the ground, the derived concentrations are similar to those observed. However, photolysis is the dominant loss mechanism at these altitudes. At 5 km above sea level, the estimated lifetimes of $CHBr_3$ due to photolysis and OH are 36 days and 100 days, respectively [*WMO*, 1999].

Figure 2

2.2.2. Inorganic bromine. The destruction of each $CHBr_3$ molecule produces three bromine atoms. Hence, the production of Br_y is related to the loss frequency of $CHBr_3$. If χ and L are the $CHBr_3$ number density and loss frequency, respectively, then the number density increase of Br_y at each time step is $3\chi[1 - 1/(1 + L\Delta t)]$. We maintain only a count of the number of bromine atoms and do not partition them among bromine-containing species.

The loss frequency for Br_y is zero in the stratosphere since the only removal mechanism is transport to the troposphere or mesosphere [*WMO*, 1999]. In the troposphere, however, it is not well established how Br_y is affected by scavenging and rain out. Since one of our objectives is to estimate the relative contributions to stratospheric Br_y from in-situ destruction of $CHBr_3$ and from transport of Br_y through the tropopause after $CHBr_3$ destruction in the troposphere, we perform two experiments. In the first experiment, called the "base case," we assume that the tropospheric lifetime of Br_y is ten days, just as do *Dvortsov et al.* [1999]. This is implemented by setting the loss frequency, L, to 2×10^{-6} sec^{-1}. In the second experiment we immediately remove all tropospheric Br_y. This constrains the remaining Br_y to be completely of stratospheric origin. The amount of stratospheric Br_y in the "base case" experiment which exceeds that in the second experiment is due to transport of Br_y from the troposphere to the stratosphere. We define the tropopause as the 380 K potential temperature surface within 10° latitude of the equator and the 2 PVU surface elsewhere [*Holton et al.*, 1995]. One potential vorticity unit (PVU) is 1×10^{-6} m^2 K kg^{-1} s^{-1}.

3. Results

3.1. Bromoform

The yearly recycling of the GEOS-DAS dynamics and the solar dependence of the photolysis and oxidation force $CHBr_3$'s mixing ratios into a repeating annual cycle during the last three years of the experiment. Figure 3 compares the zonally averaged $CHBr_3$ mixing ratios at two-month intervals. Figure 3
These panels demonstrate the strong latitudinal variance of tropospheric $CHBr_3$ and show that the amplitude of the annual cycle in the troposphere increases with latitude as is observed [*Cicerone et al.*, 1988; *WMO*, 1999] and that the phase of the annual cycle shifts by six months across the equator. This is because the emission scenario has no time dependence while the two loss mechanisms are functions of the apparent solar declination. $CHBr_3$ accumulates in the winter hemisphere because photolysis and oxidation decline while the surface emission remains unchanged. Globally, the tropospheric $CHBr_3$ burden maximizes in the southern hemisphere winter due to the larger ocean surface area.

The annual cycle of $CHBr_3$ at Hawaii during the final two years of the simulation is shown in Figure 4. Superimposed are $CHBr_3$ samples from Mauna Loa at 3.4 km altitude during four observing periods in 1991 and 1992 [*Atlas and Ridley*, 1996]. Mauna Loa is regarded as residing in the free troposphere away from significant coastal upwelling. Figure 4 demonstrates that despite the simple nature of the surface emission scenario the PCTM generates mixing ratios that are close to those observed at this site. The seasonal dependence of the variance of $CHBr_3$, larger in winter, is also reproduced. Figure 4

Using equatorial data, Figure 5 provides a comparison of $CHBr_3$ in the equatorial troposphere and lower stratosphere of the PCTM with data from the August and September 1996 Pacific Exploratory Mission-Tropics (PEM-Tropics) [*Schauffler et al.*, 1999]. Included also are observations from the 1996 Stratospheric Tracers of Atmospheric Transport (STRAT) Campaign within 30° of the Equator. The PCTM data are taken from August and September. The PCTM's mixing ratios are larger than observed in the troposphere above 10 km and in the first few kilometers above the tropopause (380 K). As in *Dvortsov et al.* [1999], the excess in the upper troposphere is attributed to convection, which appears to be extracting too much $CHBr_3$ from the lower troposphere and the boundary layer and depositing it in the upper troposphere. Indeed, *Allen et al.* [1997] find that the frequency of tropical convection in GEOS-DAS is overestimated. However, they also note that the average cloud top pressures of the modeled convection near the equator, approximately 240 hPa, are comparable to International Satellite Cloud Climatology (ISCCP) [*Rossow et al.*, 1996] cloud top pressures. Figure 5

In the lower tropical stratosphere the elevated $CHBr_3$ mixing ratios are most likely due to the rapid vertical transport seen by *Strahan et al.* [1998] and *Gettelman et al.* [2000] in their simulations using GEOS-DAS winds, and by *Hall et al.* [1999] in their intercomparison of stratospheric models. Attributed to the mean meridional circulation, it is responsible for the rapid vertical propagation of the so-called tape recorder signal [*Mote et al.*, 1996] in both water vapor and CO_2. We see similar propagation speeds (not shown) in our CO_2 experiment. Thus, the convective parameterization is not the direct cause of the excessive tropical lower stratospheric $CHBr_3$. Rather, the high frequency of convection is generating anomalously high mixing ratios in the tropical upper troposphere which

serve as the lower boundary condition for vertical transport through the tropical tropopause by the mean circulation. The primary impact of the resulting high bias in tropical $CHBr_3$ is a proportional overestimation of the amount of stratospheric in-situ production of Br_y from the tropopause to approximately 20 kilometers in the tropical stratosphere.

In the middle latitudes, quasi-horizontal isentropic cross-tropopause transport and downward vertical advection from the stratospheric overworld are the two dominant pathways by which the composition of air in the lowermost stratosphere is controlled [*Holton et al.*, 1995]. Figure 6 illustrates the zonally averaged $CHBr_3$ mixing ratio on the 360K isentropic surface from the equator to 60° N. This surface lies in the upper troposphere at low latitudes and in the lowermost stratosphere at high latitudes. In the middle-latitudes, the mixing ratios oscillate with time reflecting the seasonal dependence of the transport. From vernal to autumnal equinox, the time of year when photochemical destruction is the strongest, mixing ratios grow as enough tropospheric air is transported isentropically across the tropopause into the stratosphere to offset the chemical loss. At autumnal equinox, the trend of the mixing ratios reverses. Photochemical loss, weaker now than during summer, but not zero, conspires with the onset of downward transport from the overworld to force the mixing ratios to decline. Figure 7 illustrates the zonally averaged (Eulerian) vertical wind speed at 380K as diagnosed by the PCTM's transport algorithm. The vertical wind speed is most strongly negative during the winter months and is not significantly different from zero in the summer months. The above diagnostics demonstrate that outside of the deep tropics GEOS-DAS simulates the dominant observed large-scale transport mechanisms near and along the tropopause.

Figure 6

Figure 7

3.2. Inorganic bromine

The zonally averaged Br_y mixing ratio at the conclusion of four years' integration of the base case (tropospheric Br_y 10-day lifetime) is illustrated in Figure 8a. In the PCTM, $CHBr_3$'s stratospheric contribution maximizes generally several kilometers above the tropopause. Over the equator, this is between 20 and 25 km where our mixing ratios peak at 1.1 pptv. In the middle latitudes at 20 km,

Figure 8

Dvortsov et al. [1999] show a peak of 1.8 pptv. In the troposphere our equatorial Br_y mixing ratios more closely resemble those of *Dvortsov et al.* [1999]. For comparison, Figure 8b shows the zonally averaged Br_y mixing ratio from the FCTM. In contrast to the Br_y which is produced from destruction of $CHBr_3$ and the other short-lived compounds, the contribution of the long-lived compounds is greatest in the middle and upper stratosphere and accounts for Br_y mixing ratios of approximately 14 parts per trillion by volume (pptv) at 10 hPa. Near the tropopause, Br_y in the FCTM is generally near 1 pptv and is much less in most of the troposphere.

Since the smallest contribution to stratospheric Br_y mixing ratios from the long-lived sources is in the lowest stratosphere, $CHBr_3$ makes its largest relative contribution to Br_y just above the tropopause. To illustrate, we integrate upward from the tropopause and determine the global mass of Br_y as a function of the number of grid boxes above the tropopause. The winds driving each transport model are identical, so the location of the of the tropopause is the same in each experiment. The vertical discretization of the FCTM is coarser than that of the PCTM, so we interpolate the FCTM's Br_y onto the PCTM's levels. The results of this tropopause-following upward integration for the final day of the four-year PCTM experiment are shown in Figure 9a along with the results from the FCTM for January 1, 1998, the same calendar day. In the set of grid boxes which lie immediately above the tropopause, Br_y produced from the loss of $CHBr_3$ in the PCTM amounts to approximately 45% of that which is produced from the loss of the long-lived brominated compounds in the FCTM, or about one-third of the total. As more overlaying grid boxes are included in the vertical integration, the proportion falls reflecting the increasing dominance of Br_y from the long-lived compounds in the middle and upper stratosphere.

Figure 9

Figure 9b presents the seasonal variation of the ratio of PCTM- to FCTM-Br_y during the final eight months of the four-year PCTM experiment. The individual curves represent the ratio for the entire stratosphere and for the first layer of grid boxes above the tropopause from pole-to-pole and from 15° and 60° north latitude. During the northern summer just above the tropopause, the ratio in the northern middle latitudes rises from approximately 0.30 in June to 0.45 in October. This suggests that

tropospheric air, relatively rich in Br_y with respect to stratospheric air in the PCTM, but relatively poor in Br_y with respect to stratospheric air in the FCTM, is being transported isentropically from the troposphere to the northern lowermost stratosphere. Shortly after autumnal equinox, the fraction begins to fall as the circulation switches to the winter regime. Transport from aloft brings smaller mixing ratios of Br_y into the northern lowermost stratosphere of the PCTM and higher mixing ratios of Br_y into the northern lowermost stratosphere of the FCTM. This seasonal variation reflects the characteristics of the circulation discussed in the Section 3.1. The seasonal variation of the ratio obtained when considering all first-layer lower stratospheric grid boxes indicates that the results presented in Figure 9a are representative of the annual average. This diagnostic does not support the hypothesis of *Dvortsov et al.* [1999] that $CHBr_3$ could contribute more Br_y in the lowermost stratosphere than all the long-lived sources combined.

Accounting for the entire stratosphere, we estimate that adding $CHBr_3$ to models which already contain the long-lived brominated compounds will increase the simulated stratospheric Br_y by approximately 15%. We consider this an upper bound because of the excessive $CHBr_3$ mixing ratios in the lower equatorial stratosphere of the PCTM.

Figure 10 illustrates the evolution of the globally integrated stratospheric mass of Br_y from both PCTM experiments (tropospheric Br_y 10-day lifetime and immediate tropospheric rain out). The relative contributions to stratospheric Br_y due to in-situ production and to transport from the troposphere are derived by comparing the two cases. Their difference represents the amount of Br_y transported into the stratosphere after it is produced by photolysis and oxidation of $CHBr_3$ in the troposphere. Our lack of knowledge of the scavenging microphysics of the several molecules which are end products of tropospheric $CHBr_3$ destruction makes the estimate of mass transported from the troposphere uncertain. In this simulation, the relative contributions to stratospheric Br_y are comparable, but the amounts transported from the troposphere may vary strongly with other parameterizations of rain out. After integrating the PCTM for four years, the mass of Br_y is approaching a steady state and, with the uncertainties in mind, integrating further will not change the results of this study. These

Figure 10

experiments show that transport from the troposphere may indeed represent a source of stratospheric Br_y as postulated by *Ko et al.* [1997].

4. Summary and Conclusion

The Goddard three-dimensional PCTM is used to simulate $CHBr_3$ and its contribution to stratospheric inorganic bromine. $CHBr_3$ is parameterized as an ocean surface source gas with loss due to photolysis and reaction with OH in the troposphere and stratosphere. Br_y is produced from the loss of $CHBr_3$. A parameterization of convection is included and is necessary to transport $CHBr_3$ to the upper troposphere. The PCTM is integrated for four years using GEOS-DAS assimilated winds, and at the end of the experiment Br_y is approaching a steady state.

Several features of the observed distribution of $CHBr_3$ are simulated well. These include a strong vertical gradient within 2 km of the ground, mixing ratios near 0.5 pptv in the free troposphere at the equator, larger tropospheric mixing ratios in the winter hemisphere, and a seasonal cycle which is realistic at Mauna Loa and whose amplitude increases with latitude. The most important shortcoming of the comparison of the PCTM's $CHBr_3$ with the limited set of observations is the presence of $CHBr_3$ mixing ratios about a factor of two greater than observed in the lowest five kilometers of the equatorial stratosphere. We discount the cause as convection since the cloud top heights from the GEOS-DAS assimilation are not stratospheric. Instead, the cause is vertical advection driven by the GEOS-DAS residual mean circulation which is known from previous studies to be too strong in the tropical lower stratosphere. At middle and high latitudes, the observed seasonal variation of the composition of air in the lowermost stratosphere is qualitatively simulated, indicating that the dominant transport mechanisms, downward vertical transport from the overworld and cross-tropopause isentropic transport from the tropical troposphere to the stratosphere, are controlling the $CHBr_3$ mixing ratios. In fact, transport dominates chemical loss in the summer lowermost northern stratosphere because the mixing ratios increase during the period of strongest photolysis.

We use a tropopause-following method of calculating the mass of stratospheric Br_y attributable to

the photolysis and oxidation of $CHBr_3$. We estimate that in the first kilometer above the tropopause, the contribution of $CHBr_3$ to the mass of Br_y averages approximately 45% of that comes from the long-lived organic brominated compounds, or about one-third of the total. The seasonal variation is 33% to 54%. With our choice of parameterizations, we estimate that the mass of Br_y transported through tropopause which originates from $CHBr_3$ destruction in the troposphere is comparable to the mass produced from $CHBr_3$ destruction within the stratosphere. Both components of this estimate are uncertain. The high bias in equatorial lower stratospheric $CHBr_3$ likely makes our estimate of the in-situ contribution to Br_y an upper bound. We also do not partition the released bromine into the individual molecules that comprise Br_y and do not parameterize the details of Br_y microphysics and scavenging. We estimate that adding $CHBr_3$ to models which already include the long-lived brominated compounds will increase the simulated stratospheric mass of Br_y by about 15%.

This study suggests that the short-lived organic brominated compounds make a contribution to stratospheric inorganic bromine which should not be neglected. However, our results are different from those of *Dvortsov et al.* [1999] because globally at no level in the stratosphere is $CHBr_3$'s contribution to stratospheric Br_y greater than that from the long-lived compounds, even in the first few kilometers above the tropopause where the relative magnitude of the contribution from $CHBr_3$ is the greatest. While future observations will make it possible to constrain the chemical parameterizations and improved representations of convection can be expected, these processes do not represent the major difference between these experiments and those of *Dvortsov et al.* [1999]. Rather, the three-dimensional character of these experiments allows us to determine the location of the tropopause over the entire globe and to consistently separate stratospheric from tropospheric air. In addition, we use observations of other photolytic species to validate the observed transport mechanisms in the lowermost stratosphere. Each of these elements of the analysis lend confidence to the results and demonstrate how inferences of ozone trends critically depend on the representation of the large-scale transport, especially in the lowermost stratosphere.

Acknowledgments. We thank Eric Fleming for providing the monthly zonal averages of [OH] and

photolysis loss frequency for $CHBr_3$. This is contribution number *nnn* from the Stratospheric General Circulation with Chemistry Project at NASA Goddard Space Flight Center.

References

Allen, D. J., K. E. Pickering, and A. Molod, An evaluation of deep convective mixing in the Goddard chemical transport model using International Satellite Cloud Climatology Project cloud parameters, *J. Geophys. Res.*, *102*, 25,467-25,476, 1997.

Appenzeller, C., J. R. Holton, and K. H. Rosenlof, Seasonal variation of mass transport across the tropopause, *J. Geophys. Res.*,*101*, 15,071-15,078, 1996.

Atlas, E. L., and B. A. Ridley, The Mauna Loa Observatory Photochemistry Experiment: Introduction, *J. Geophys. Res.*,*101*, 14,531-14,541, 1996.

Chen, P., Isentropic cross-tropopause mass exchange in the extratropics, *J. Geophys. Res.*,*100*, 16,661-16,673, 1995.

Cicerone, R. J., L. E. Heidt, and W. H. Pollock, Measurements of atmospheric methyl bromide and bromoform, *J. Geophys. Res.*, *93*, 3745-3749, 1988.

DeMore, W. B., S. P. Sander, D. M. Golden, R. F. Hampson, M. J. Kurylo, C. J. Howard, A. R. Ravishankara, C. E. Kolb, and M. J. Molina, Chemical kinetics and photochemical data for use in stratospheric modeling, Evaluation number 12. *NASA JPL Publication No. 97-4*, Jet Propulsion Laboratory, Pasadena, California, 266 pp, 1997.

Dessler, A. E., E. J. Hintsa, E. M. Weinstock, J. G. Anderson, and K. R. Chan, Mechanism controlling the water vapor in the lower stratosphere: A tale of two stratospheres, *J. Geophys. Res.*,*100*, 23,167-23,172, 1995.

Douglass, A. R., C. H. Jackman, and R. S. Stolarski, Comparison of model results transporting the odd nitrogen family with results transporting odd nitrogen species, *J. Geophys. Res.*, *94*, 9862-9872, 1989.

Douglass, A. R., and S. R. Kawa, Contrast between 1992 and 1997 high-latitude spring Halogen Occultation Experiment observations of lower stratospheric HCl, *J. Geophys. Res.*, *104*, 18,739-18,754, 1999.

Douglass, A. R., M. J. Prather, T. M. Hall, S. E. Strahan, P. J. Rasch, L. C. Sparling, L. Coy, and J. M. Rodriguez, Choosing meteorological input for the global modeling initiative assessment of high-speed aircraft. *J. Geophys. Res.*, *104*, 27,545-27,564, 1999.

Douglass, A. R., C. J. Weaver, R. B. Rood, and L. Coy, A three-dimensional simulation of the ozone annual cycle using winds from a data assimilation system, *J. Geophys. Res.*, *101*, 1463-1474, 1996.

Douglass, A. R., R. B. Rood, S. R. Kawa and D. J. Allen, A three-dimensional simulation of the evolution of the middle latitude winter ozone in the middle stratosphere, *J. Geophys. Res.*, *102*, 19,217-19,232, 1997.

Dunkerton, T. J., Evidence of meridional motion in the summer lower stratosphere adjacent to monsoon regions, *J. Geophys. Res.*,*100*, 16,675-16,688, 1995.

Dvortsov, V. L., M. A. Geller, S. Solomon, S. M. Schauffler, E. L. Atlas, and D. R. Blake, Rethinking reactive halogen budgets in the midlatitude lower stratosphere, *Geophys. Res. Lett.*, *26*, 1699-1702, 1999.

Fleming, E. L., C. H. Jackman, R. S. Stolarski, and D. B. Considine, Simulation of stratospheric tracers using and improved empirically based two-dimensional model transport formulation, *J. Geophys. Res.*, *104*, 23,911-23,934, 1999.

Gettelman, A, J. R. Holton, and A. R. Douglass, Simulations of water vapor in the lower stratosphere and upper troposphere, *J. Geophys. Res.*, *105*, 9003-9023, 2000.

Gschwend, P. M., J. K. McFarlane, K. A. Newman, Volatile halogenated organic compounds released to seawater from temperate marine macroalgae, *Science*, *227*, 1033-1035, 1985.

Hall, T. M., and M. J. Prather, Simulations of the trend and annual cycle of stratospheric CO_2, *J. Geophys. Res.*, *98*, 10,573-10,581, 1993.

Hall, T. M., D. W. Waugh, K. A. Boering, and R. A. Plumb, Evaluation of transport in stratospheric models, *J. Geophys. Res.*, *104*, 18,815-18,839, 1999.

Hintsa, E. J, et al., Troposphere to stratosphere transport in the lowermost stratosphere from measurements of H_2O, CO_2, N_2O and O_3, *Geophys. Res. Lett.*, *25*, 2655-2658, 1998.

Holton, J. R., P. H. Haynes, M. E. McIntyre, A. R. Douglass, R. B. Rood, and L. Pfister, Stratosphere-troposphere exchange, *Rev. Geophys.*, *33* 403-439, 1995.

Ko, M. K. W., N. D. Sze, C. J. Scott, and D. K Weisenstein, On the relationship between stratospheric chlorine/bromine loading and short-lived tropospheric source gases, *J. Geophys. Res.*, *102*, 25,507-25,517, 1997.

Lin, S.-J., and R. B. Rood, Multidimensional flux-form semi-Lagrangian transport schemes, *Mon. Wea. Rev.*, *124*, 2046-2070, 1996.

Liss, P. S., The air-sea exchange of low molecular weight halocarbon gases, in *The Role of Air-Sea Exchange in Geochemical Cycling*, edited by P. Buat-Menard, D. Reidel Publishing Company, 283-294, 1986.

McRea, G. J., W. R. Goodin, and J. H. Seinfeld, Numerical solution of the atmospheric diffusion equation for chemically reacting flows. *J. Comput. Phys.*, *45*, 1-42, 1982.

Moore, R., R. Tokarczyk, and C. Green, Sources of organobromines to the arctic atmosphere, in *The Tropospheric Chemistry of Ozone in the Polar Regions*, edited by H. Niki and K. H. Becker, Springer-Verlag, New York, 235-250, 1993.

Mote, P. W., K. H. Rosenlof, M. E. McIntyre, E. S. Carr, J. C. Gille, J. R. Holton, J. S. Kinnersley, H. C. Pumphrey, J. M. Russell, and J. W. Waters, An atmospheric tape recorder: The imprint of tropical tropopause temperatures on stratospheric water vapor, *J. Geophys. Res.*, *101*, 3989-4006, 1996.

Penkett, S. A., B. M. R. Jones, M. J. Rycroft, and D. A. Simmons, An interhemispheric comparison of the concentrations of bromine compounds in the atmosphere, *Nature*, *318*, 550-553, 1983.

Rasch, P. J., N. M. Mahowald, and B. E. Eaton, Representations of transport, convection, and the hydrologic cycle in chemical transport models: Implications for the modeling of short lived and soluble species, *J. Geophys. Res.*, *102*, 28,127-28,138, 1997.

Ray, E. A., F. L. Moore, J. W. Elkins, G. S. Dutton, D. W. Fahey, H. Vömel, S. J. Oltmans, and K. H. Rosenlof, Transport into the Northern Hemisphere lowermost stratosphere revealed by in situ tracer measurements, *J. Geophys. Res.*, *104*, 26,565-26,580, 1999.

Rood, R. B. Numerical advection algorithms and their role in atmospheric transport and chemistry models, *Rev. Geophys.*, *25*, 71-100, 1987.

Rood, R. B., A. R. Douglass, M. C. Cerniglia, L. C. Sparling, and J. E. Nielsen, Seasonal variability of middle-latitude ozone in the lowermost stratosphere derived from probability distribution functions, *J. Geophys. Res.*, *in press*, 2000.

Rood, R. B., A. R. Douglass, J. A. Kaye, M. A. Geller, C. Yuechen, D. J. Allen, E. M. Larson, E. R. Nash, and J. E. Nielsen, Three-dimensional simulations of wintertime ozone variability in the lower stratosphere, *J. Geophys. Res.*, *96*, 5055-5071, 1991.

Rossow, W. B., A. W. Walker, D. E. Beuschel, and M. D. Roiter, International Satellite Cloud Climatology Project (ISCCP) documentation of new cloud data sets, *WMO/TD 737*, 115 pp., World Meteorological Org., Geneva, 1996.

Schauffler, S. M., E. L. Atlas, D. R. Blake, F. Flocke, R. A. Lueb, J. M. Lee-Taylor, V. Stroud, and W.

Travnicek, Distributions of brominated organic compounds in the troposphere and lower stratosphere, *J. Geophys. Res.*, *104*, 21,513-21,535, 1999.

Schneider E. K., and R. S. Lindzen, A discussion of the parameterization of momentum exchange by cumulus convection, *J. Geophys. Res.*, *81*, 3158-3161, 1976.

Schubert, S. D., R. B. Rood, and J. Pfaendtner, An assimilated dataset for earth science applications, *Bull. Am. Meteorol. Soc.*, *74*, 2331-2342, 1993.

Smyshlyaev, S. P., V. Dvortsov, M. A. Geller, and V. A. Yudin, A two-dimensional model with input parameters from a GCM: Ozone sensitivity to different formulations for the longitude temperature variations, *J. Geophys. Res.*, *103*, 28,373-28,387, 1998.

Spivakovsky, C. M., J. A. Logan, S. A. Montzka, Y. J. Balkanski, M. Foreman-Fowler, D. B. A. Jones, L. W. Horowitz, A. C. Fusco, C. A. M. Brenninkmeijer, M. J. Prather, S. C. Wofsy, and M. B. McElroy, Three-dimensional climatological distribution of tropospheric OH: Update and evaluation, *J. Geophys. Res.*, *105*, 8931-8980, 2000.

Strahan, S. E., A. R. Douglass, J. E. Nielsen, and K. A. Boering, The CO_2 seasonal cycle as a tracer of transport, *J. Geophys. Res.*, *103*, 13,729-13,741, 1998.

Sturges, W. T., G. F. Cota, and P. T. Buckley, Bromoform emission from ice algae, *Nature*, *358*, 660-662, 1992.

World Meteorological Organization (WMO), Scientific Assessment of Ozone Depletion: 1998, *Rep. No. 44*, Global Ozone Res. and Monitoring Proj., Geneva, 1999.

J. E. Nielsen, Emergent Information Technologies, Inc., Code 916, NASA Goddard Space Flight Center, Greenbelt, MD 20771. (e-mail: eric.nielsen@gsfc.nasa.gov)

A. R. Douglass, Code 916, NASA Goddard Space Flight Center, Greenbelt, MD 20771. (e-mail: douglass@persephone.gsfc.nasa.gov)

Received _____

[1]Also at NASA Goddard Space Flight Center, Greenbelt, Maryland

Figure captions

Figure 1. Zonally averaged CO_2 mixing ratio (ppmv) at 60° N latitude from the upper troposphere (black) and the lower stratosphere (gray) during the second year of the two-year CO_2 simulation.

Figure 2. PCTM daily average OH number density on the Equator at equinox (solid) and equatorial tropospheric OH number densities from *Spivakovski et al.* [2000] (dashed).

Figure 3. Zonally averaged $CHBr_3$ mixing ratio (pptv) at two month intervals. Contour interval is 0.25 pptv to 2 pptv, 1 pptv thereafter. The annual cycle is identical in the final three years of the four-year experiment. Isentropes (dashed lines) at 20 K intervals from 320 K to 400 K are provided for reference.

Figure 4. $CHBr_3$ mixing ratio (pptv) at one-day intervals at Hawaii from the PCTM and the Mauna Loa observations at 3.4 km altitude from *Atlas and Ridley* [1996]. Error bars delineate one standard deviation.

Figure 5. $CHBr_3$ profiles at 2° S latitude from PEM-Tropics (dashed), from the PCTM in August and September (solid), and from 1996 STRAT ER2 flights within 30° latitude of the equator (triangles). Error bars delineate one standard deviation.

Figure 6. Evolution of the zonally averaged $CHBr_3$ mixing ratio (pptv) along the 360K isentropic surface in the northern hemisphere during the final two years of the simulation.

Figure 7. Zonally averaged GEOS-DAS vertical wind speed (cm sec^{-1}) for 1997, used for each of the four years of the integration. Contour interval 0.1 cm sec^{-1}, negative areas shaded.

Figure 8. (top) Zonally averaged Br_y (ppmv) at the end of the PCTM's four-year integration. Contour interval 0.1 ppmv. (bottom) Zonally averaged Br_y (ppmv) from the FCTM after interpolation onto PCTM vertical discretization on the same calendar day (1 Jan 1998) in the GEOS-DAS assimilation. Contour interval varies.

Figure 9. (a) Stratospheric mass of Br_y (10^6 kg) integrated through the ten layers of grid boxes which lie at and immediately above the tropopause. FCTM in light gray and PCTM in dark gray. The three-dimensional Br_y fields used in this calculation are shown in zonal average in Figure 8. The lower abscissa provides an approximation of the elevation above the tropopause in km. (b) Ratio of Br_y in the PCTM to Br_y in the FCTM (dark solid) in the first layer of grid boxes above the tropopause for 90° S to 90° N, (light solid) in the first layer of grid boxes above the tropopause for 15° N to 60° N, and (dark-dashed) for all stratospheric grid boxes.

Figure 10. Evolution of the stratospheric mass of Br_y from the base case with tropospheric lifetime set to ten days (solid) and the case with tropospheric lifetime set to zero days (dashed). The difference (dot-dashed) represents the amount of Br_y which is transported into the stratosphere after $CHBr_3$ destruction in the troposphere. Thick lines are a Gaussian fit the individual time series (thin).

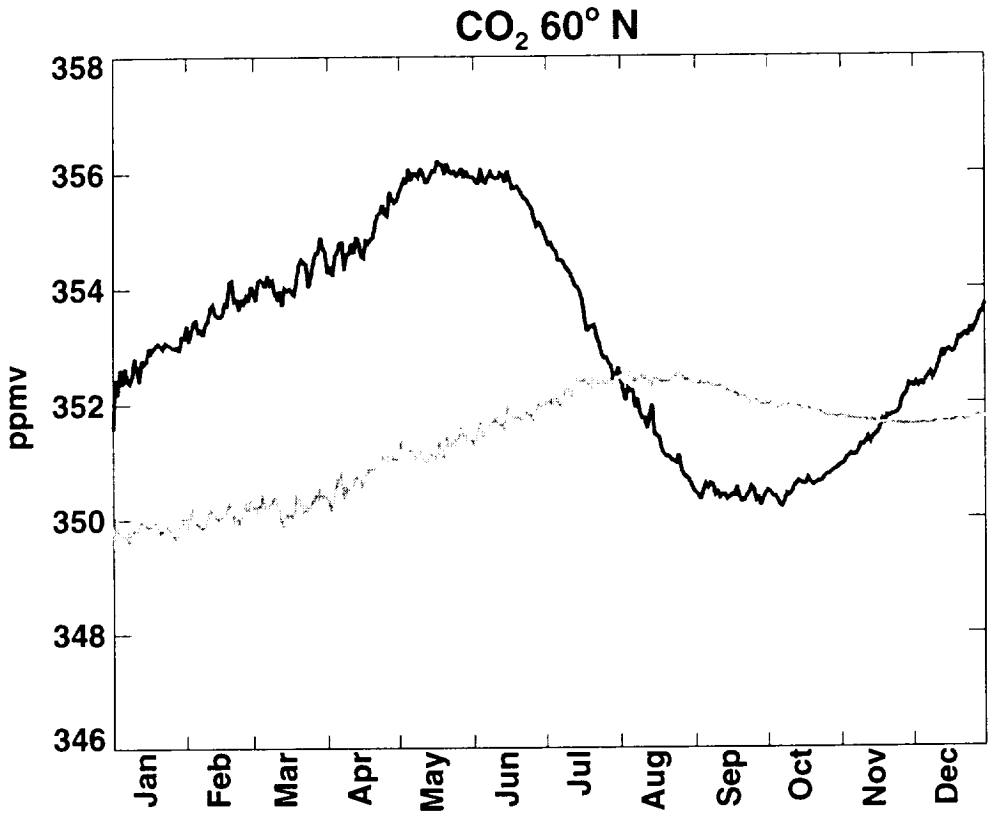
CO_2 60° N
ppmv
358
356
354
352
350
348
346
Jan
Feb
Mar
Apr
May
Jun
Jul
Aug
Sep
Oct
Nov
Dec

Figure 1

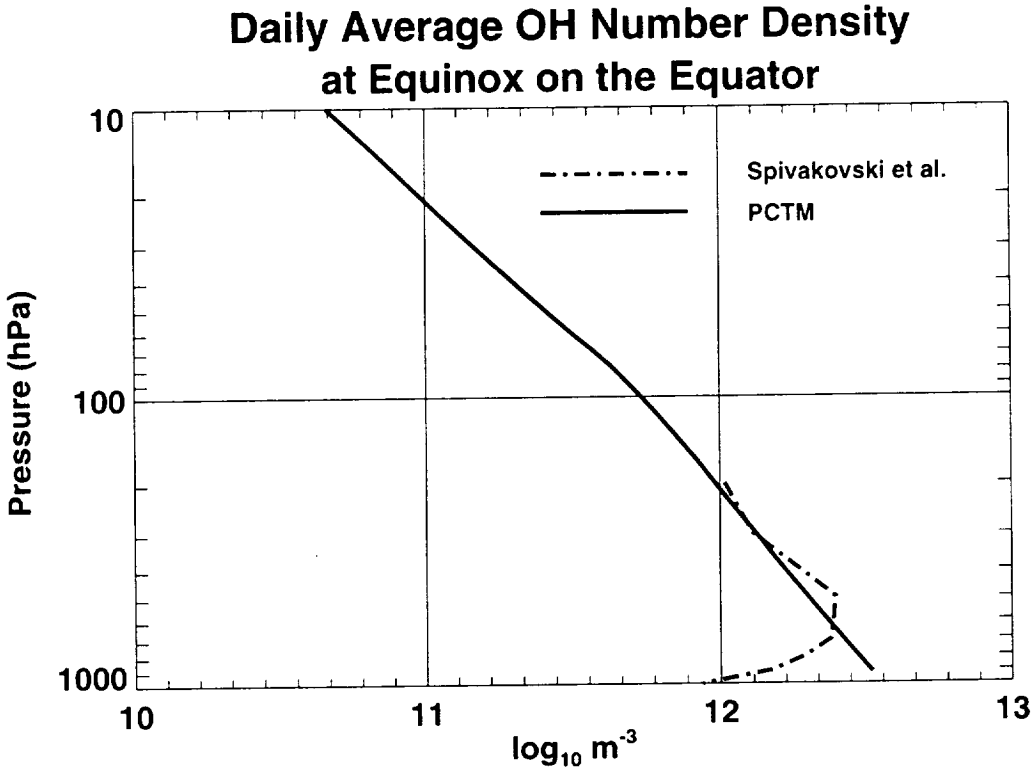
Daily Average OH Number Density
at Equinox on the Equator
Spivakovski et al.
PCTM
Pressure (hPa)
10
100
1000
10
11
12
13
log10 m-3

Figure 2

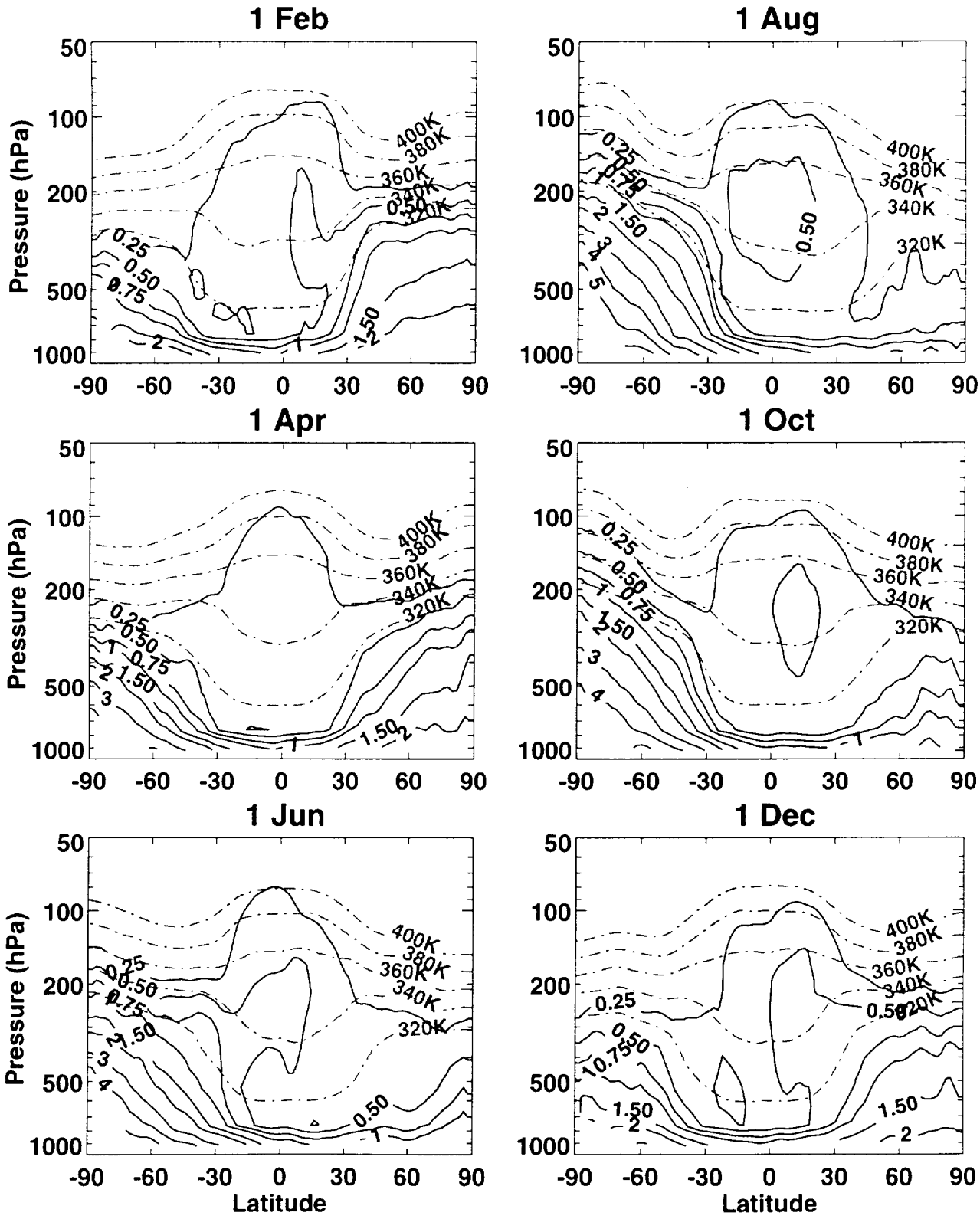
CHBr3 (pptv)
1 Feb
1 Aug
1 Apr
1 Oct
1 Jun
1 Dec
Pressure (hPa)
Latitude
50
100
200
500
1000
-90
-60
-30
0
30
60
90
400K
380K
360K
340K
320K
0.25
0.50
0.75
1.50
1
2
3
4
5

Figure 3

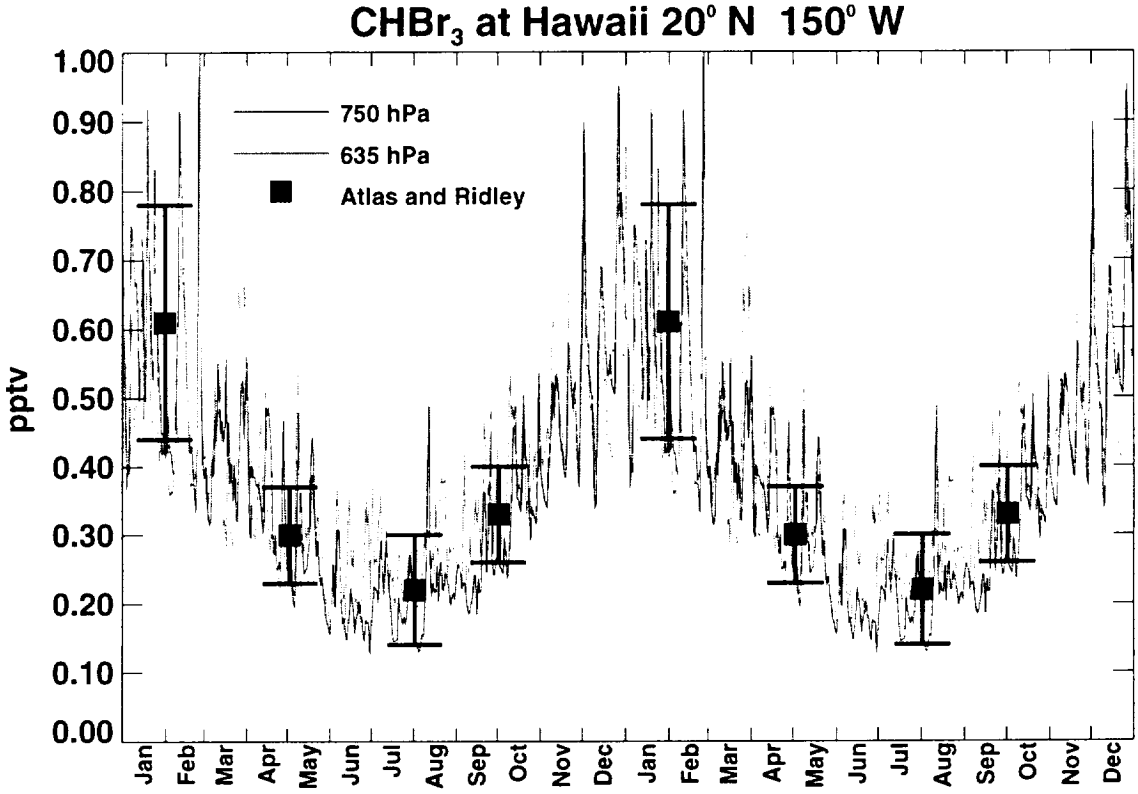
CHBr3 at Hawaii 20° N 150° W
750 hPa
635 hPa
Atlas and Ridley
pptv
1.00
0.90
0.80
0.70
0.60
0.50
0.40
0.30
0.20
0.10
0.00
Jan
Feb
Mar
Apr
May
Jun
Jul
Aug
Sep
Oct
Nov
Dec
Jan
Feb
Mar
Apr
May
Jun
Jul
Aug
Sep
Oct
Nov
Dec

Figure 4

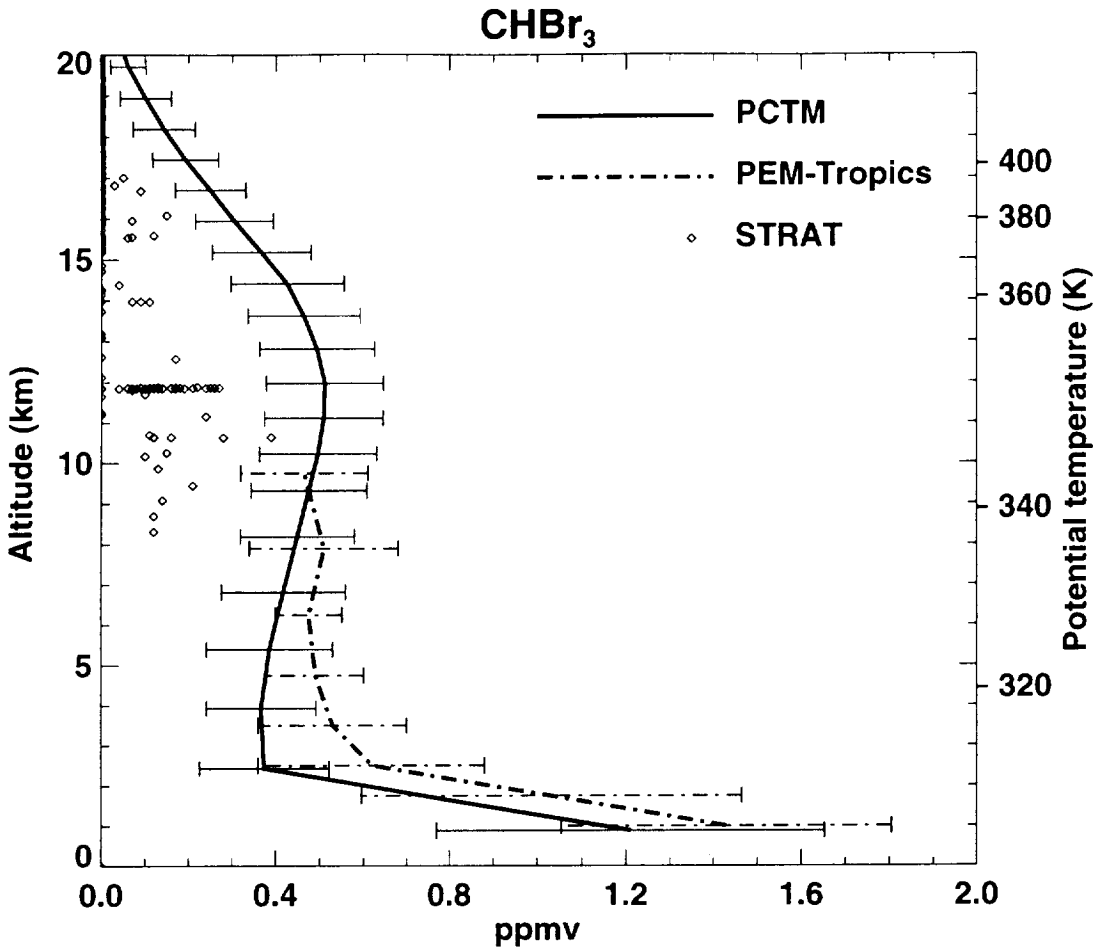
CHBr3
PCTM
PEM-Tropics
STRAT
Altitude (km)
Potential temperature (K)
ppmv
0
5
10
15
20
320
340
360
380
400
0.0
0.4
0.8
1.2
1.6
2.0

Figure 5

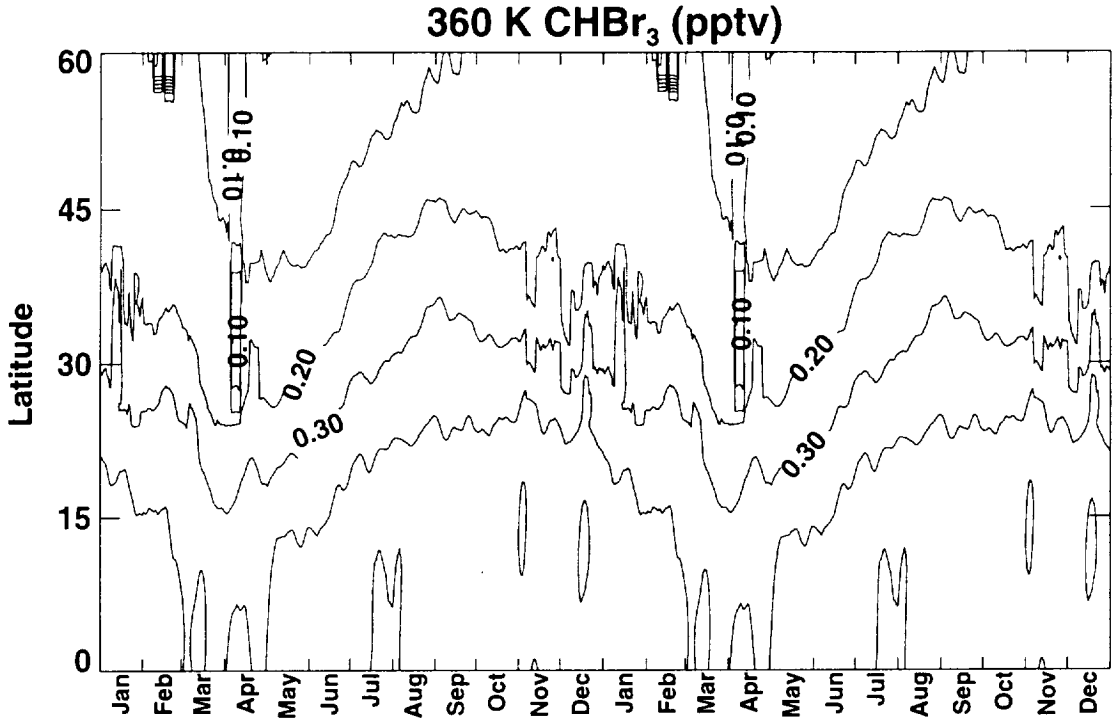
360 K CHBr3 (pptv)
Latitude
60
45
30
15
0
0.10
0.20
0.30
Jan
Feb
Mar
Apr
May
Jun
Jul
Aug
Sep
Oct
Nov
Dec

Figure 6

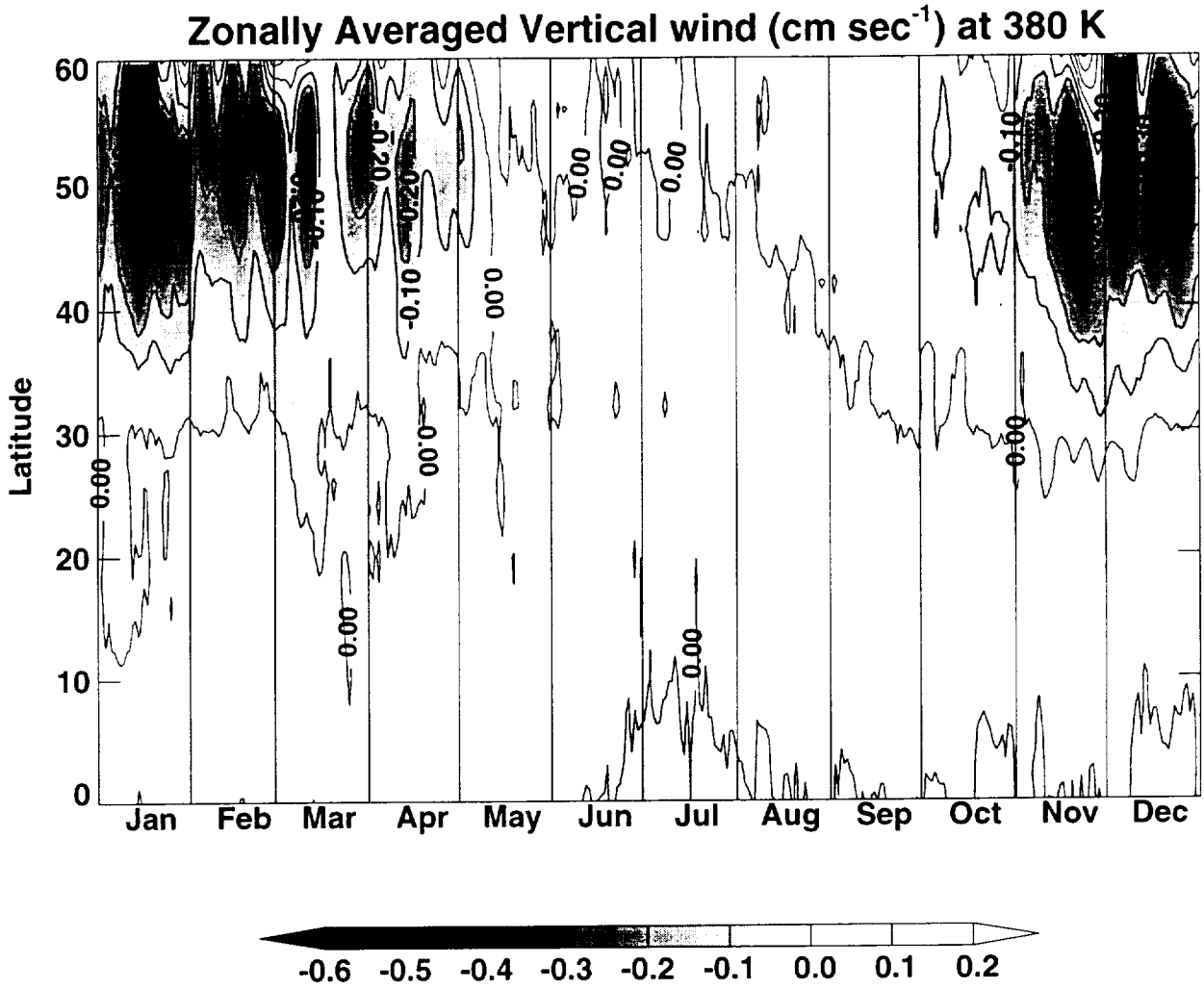
Zonally Averaged Vertical wind (cm sec-1) at 380 K
Latitude
60
50
40
30
20
10
0
Jan
Feb
Mar
Apr
May
Jun
Jul
Aug
Sep
Oct
Nov
Dec
-0.6
-0.5
-0.4
-0.3
-0.2
-0.1
0.0
0.1
0.2

Figure 7

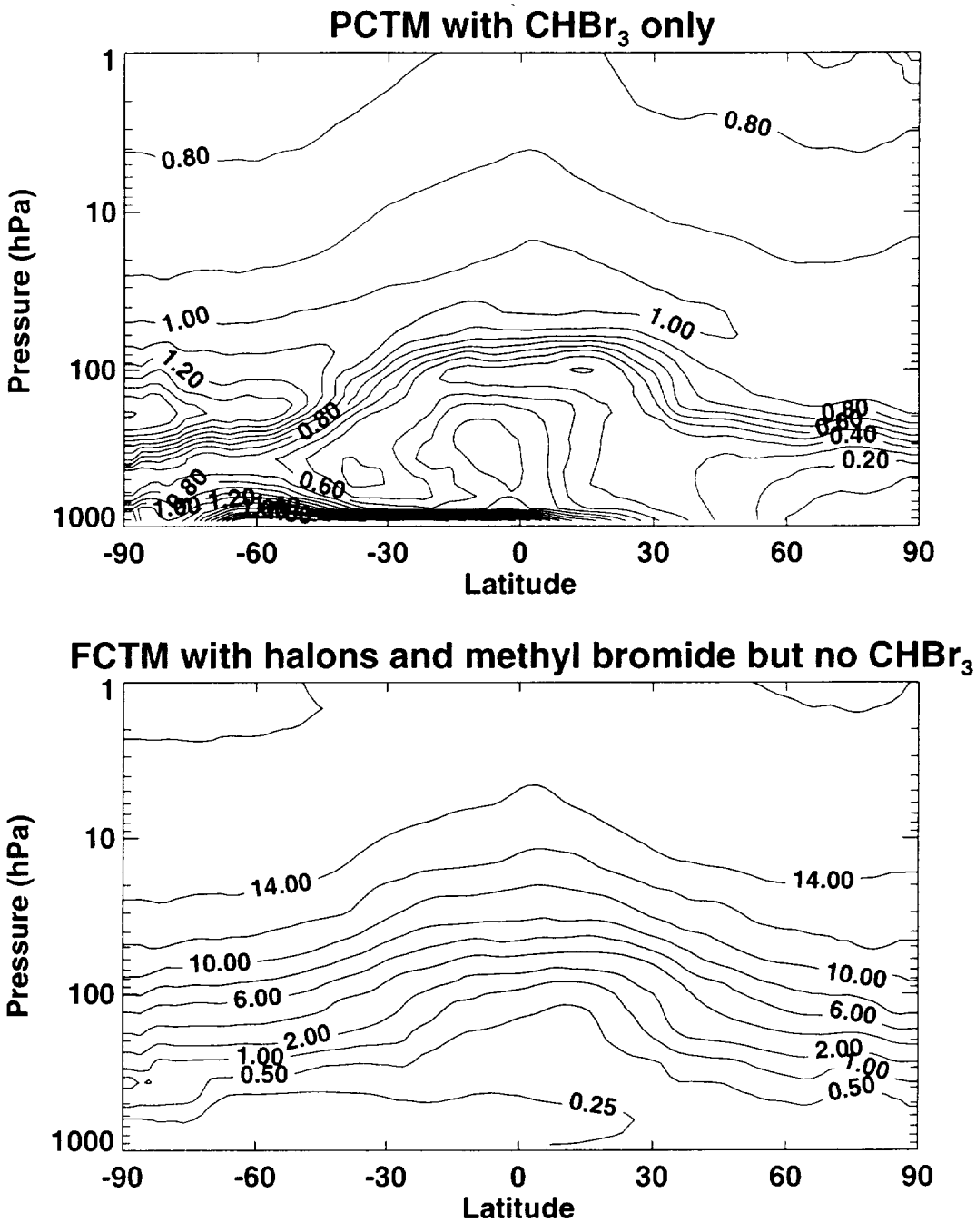
PCTM with CHBr3 only
Pressure (hPa)
1
10
100
1000
0.80
1.00
1.20
0.60
0.40
0.20
-90
-60
-30
0
30
60
90
Latitude
FCTM with halons and methyl bromide but no CHBr3
Pressure (hPa)
14.00
10.00
6.00
2.00
1.00
0.50
0.25
Latitude

Figure 8

(a)

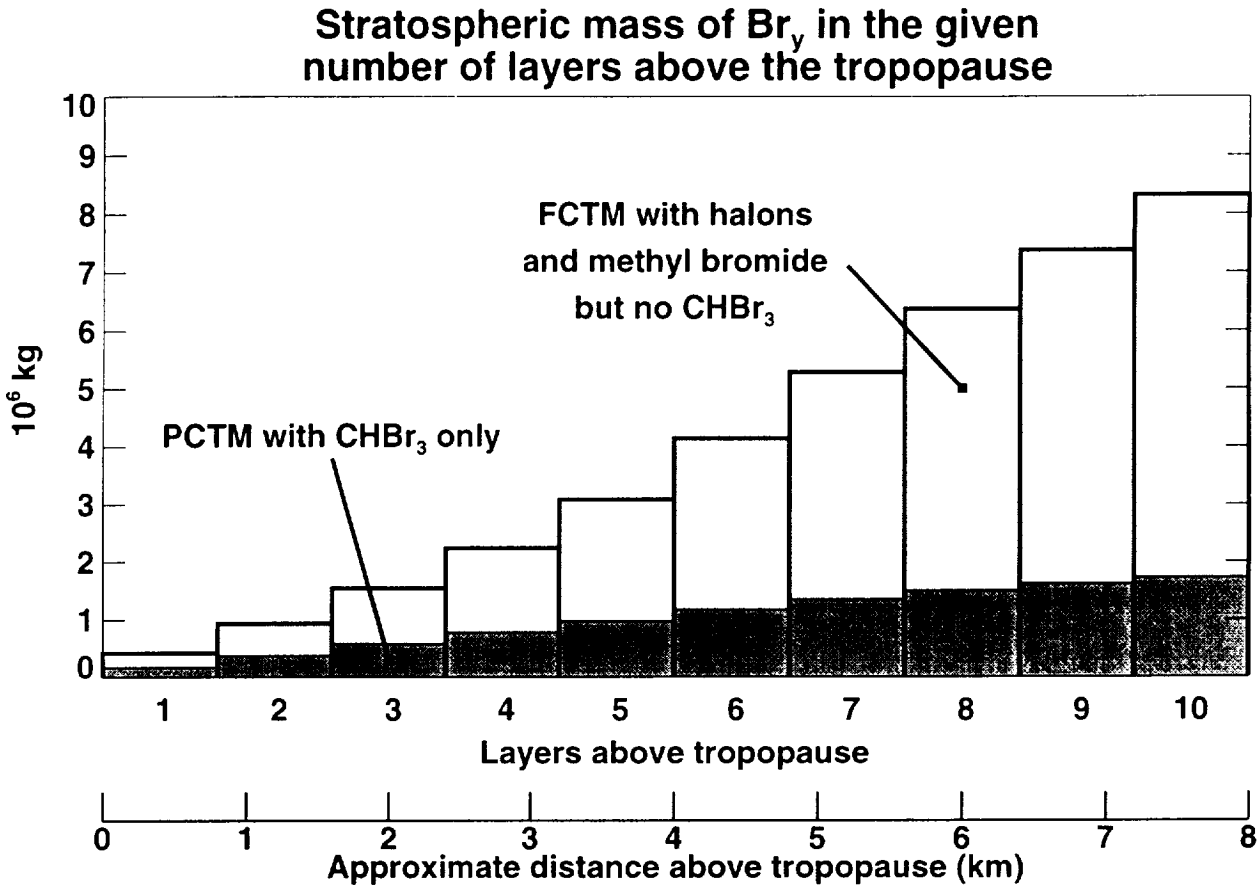
Stratospheric mass of Br_y in the given number of layers above the tropopause
10^6 kg
FCTM with halons and methyl bromide but no $CHBr_3$
PCTM with $CHBr_3$ only
Layers above tropopause
Approximate distance above tropopause (km)

(b)

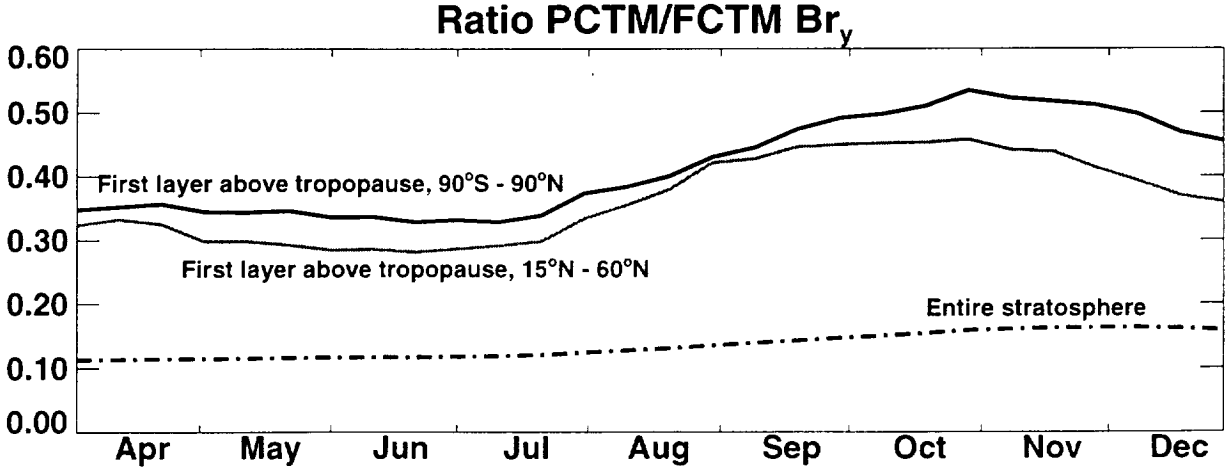
Ratio PCTM/FCTM Br_y
First layer above tropopause, 90°S - 90°N
First layer above tropopause, 15°N - 60°N
Entire stratosphere
Apr
May
Jun
Jul
Aug
Sep
Oct
Nov
Dec

Figure 9

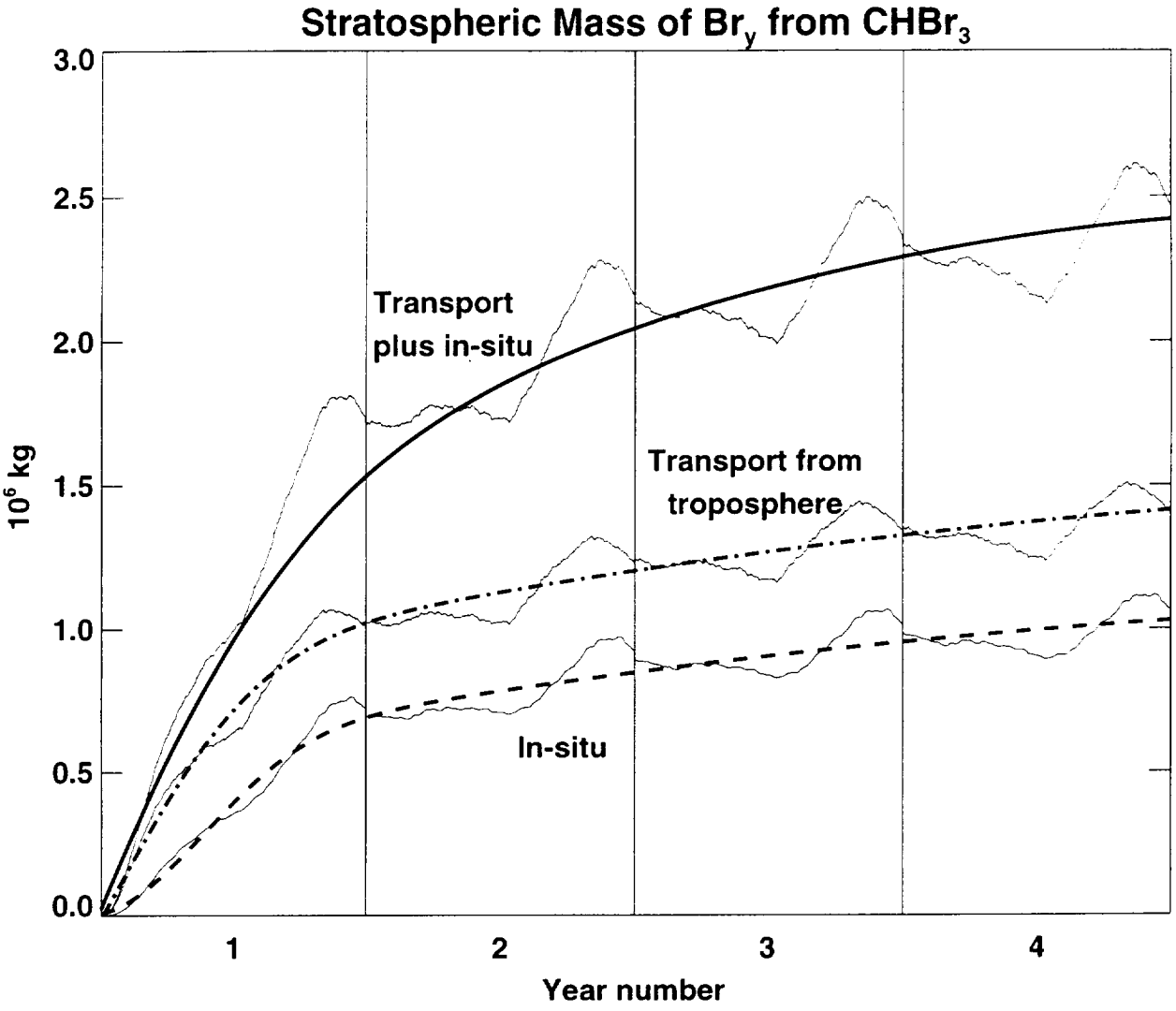
Stratospheric Mass of Br_y from $CHBr_3$
3.0
2.5
2.0
1.5
1.0
0.5
0.0
10^6 kg
Transport
plus in-situ
Transport from
troposphere
In-situ
1
2
3
4
Year number

Figure 10